Direct Comparison of Viking 2.3-GHz Signal Phase Fluctuation and Columnar Electron Density Between 2 and 160 Solar Radii

A. L. Berman
TDA Mission Support Office

J. A. Wackley
TDA Engineering Office

W. H. Hietzke
TRW Corporation

The relationship between solar wind induced signal phase fluctuation and solar wind columnar electron density has been the subject of intensive analysis during the last two decades. In this article, a sizeable volume of 2.3-GHz signal phase fluctuation and columnar electron density measurements separately and concurrently inferred from Viking spacecraft signals are compared as a function of solar geometry. These data demonstrate that signal phase fluctuation and columnar electron density are proportional over a very wide span of solar elongation angle.

A radially dependent electron density model which provides a good fit to the columnar electron density measurements and, when appropriately scaled, to the signal phase fluctuation measurements, is given as $N_e(r) = 2.21 \times 10^8\, r^{-6} + 1.55 \times 10^6\, r^{-2.3}$, *where* r = *heliocentric distance in solar radii and* $N_e(r)$ = *electron density in* cm^{-3}. *This model is also in good agreement with K-coronameter observations at 2 solar radii* ($2r_0$), *with pulsar time delay measurements at* $10r_0$, *and with spacecraft in situ electron density measurements at 1 AU.*

I. Introduction

During the last two decades, solar wind electron density and density fluctuation have been extensively investigated and analyzed via a wide variety of direct and indirect techniques. Although a number of studies have been performed using in situ spacecraft measurements at approximately 1 AU (e.g., Refs. 1-3), the very interesting regions close to the Sun were and continue to be inaccessible to spacecraft in situ measurements, and hence can only be probed indirectly via effects on observed signals which pass through or originate in these near-Sun regions.

In the early to mid 1960s, solar wind electron density fluctuation experiments focused on measurement of the

angular broadening of compact natural radio sources and subsequent modeling of this parameter as a function of solar elongation angle (Refs. 4-6). In the latter 1960s the emphasis shifted to measurement of signal intensity fluctuation in the form of the "scintillation index m" of natural radio sources (Refs. 7-11). Later studies (Refs. 12-16) emphasized the determination of the solar elongation angle (or radial) dependence of the scintillation index. More recently obtained monochromatic source spacecraft signal scintillation measurements are given in Ref. 17. Very recently, near-Sun spacecraft monochromatic signal spectral broadening has been studied (Refs. 18-20).

In the early attempts to formulate a theoretical basis for natural source intensity scintillation, it was necessary to consider signal phase fluctuation induced by electron density fluctuation. Studies which investigated the geometric dependence of signal phase fluctuation include Refs. 7, 9, 10, 14, and 21. It is, of course, not possible to directly measure phase fluctuation for noncoherent natural radio sources, as is easily done with coherent (e.g., spacecraft) signals. Additionally, the scintillation index of fluctuations from natural sources saturates of the more interesting small solar elongation angles as a result of the finite source size, whereas the monochromatic signal phase fluctuation is not subject to such an effect in this region. During the period (late 1960s, early 1970s) when the study of natural source intensity scintillation was widespread, extremely valuable (monochromatic) near-Sun spacecraft phase fluctuation data was routinely being acquired by the National Aeronautics and Space Administration (NASA)/Jet Propulsion Laboratory (JPL) Deep Space Network for other purposes (primarily tracking system performance monitoring), but was not utilized in the investigation of solar wind density fluctuation.

The first usages of single-frequency spacecraft data to probe the solar corona and solar wind consisted of a spectral broadening experiment with Mariner IV (Ref. 22), range experiments with Mariner 6 and Mariner 7 (Ref. 23), and a Mariner 6 and Mariner 7 experiment utilizing a group-phase technique (Ref. 24). However, the first investigation of solar wind density turbulence which utilized single-frequency spacecraft signal phase fluctuation was an analysis of the 1975 solar conjunction data of the Helios 1, Pioneer 10, and Pioneer 11 spacecraft (Refs. 25, 26). Results of this and subsequent investigations (Refs. 27-30) strongly suggested that signal phase fluctuation is radially proportional to columnar electron density.

This paper presents a direct comparison of concurrent spacecraft signal phase fluctuation and columnar electron density measurements obtained during the 1976 Viking solar conjunction. The data argue in favor of radial proportionality between signal phase fluctuation and columnar electron density.

II. Data

The data presented in this paper were generated during July through December 1976. During this period the two Viking Orbiter spacecraft underwent solar conjunction with a minimum Sun-Earth-Spacecraft angle of approximately 0.25 deg reached on November 26, 1976. The daily rate of change of the Sun-Earth-Spacecraft angle was approximately 0.3 deg, with the Sun-Earth-Spacecraft angle at the beginning of July being 47 deg, and 10 deg at end of December. During this entire conjunction period, the NASA-JPL Deep Space Network (DSN) maintained essentially continuous coherent communications links with both spacecraft. The ground-transmitted ("uplink") wavelength to the spacecraft was 13 cm (2.1 GHz, S-band). While the spacecraft-transmitted ("downlink") wavelengths were 13 and 3.6 cm (8.4 GHz, X-band).

During these tracking periods the DSN generates frequent measurements of doppler data (accumulated doppler phase) and less frequent measurements of spacecraft range (signal time delay). The doppler frequency referred to here is that frequency component arising from the relative motion of the spacecraft with respect to the ground antenna. These data are used for both navigation (except at small solar offset distances) and radio science (primarily at small solar offset distances). The doppler data are generated by comparing a very precise (5×10^{-14} stability over a day) ground reference frequency to the received frequency. This received frequency is simply the (ground) transmitted carrier frequency (S-band only, 2.1 GHz) which has been received, coherently multiplied (by 240/221 at S-band, 880/221 at X-band), and retransmitted by the spacecraft.

In the course of generating these data, the DSN automatically calculated low-frequency ($\sim 10^{-3}$ Hz) S-band phase fluctuation information for purposes of system performance monitoring. In the algorithm used during this time period, a fixed number (usually 15) of doppler frequency samples (usually 60-second averages) were first differenced with the predicted doppler frequency which is generated by the navigational orbit determination process. A rms doppler frequency fluctuation ("noise") was then computed after fitting with a least squares linear curve fit to remove any possible trajectory (i.e., low-frequency) errors.

A numerical simulation of the computational algorithm used (Ref. 31) provides an approximate relationship between

rms doppler phase fluctuation ϕ and rms doppler frequency fluctuation σ_d:

$$\phi(\tau) \approx 1.67\,\tau \cdot \sigma_d(\tau)$$

where

τ = doppler averaging time.

Typically, a DSN ground station generates frequent doppler measurements over a daily period of approximately 4 to 8 hours, referred to as a "tracking pass." The doppler noise data discussed in this paper have been computed in Hz as described previously in this section, and then averaged over a tracking pass to produce a single composite value ("pass average") for each daily tracking period. These Viking doppler noise data have already been extensively analyzed (Refs. 27, 28) and a more detailed explanation of the method of computation appears in Ref. 31.

The DSN generates precision (1.7 m) range (time delay) data via the modulation of a sequential binary coded signal onto the same carrier frequency described previously. At the spacecraft the range code is demodulated, and the carrier signal is coherently multiplied and remodulated with the range code and retransmitted by the spacecraft to the receiving station. The received S- and X-band range codes are compared to a reference range code which has been modulated with the extracted doppler frequency. The spacecraft range is extracted from this comparison. Appropriately multiplying and differencing the S- and X-band measurements immediately results in a direct measurement of columnar electron density (Ref. 32). Beneficially, all nonfrequency dependent effects are differenced out in this process.

The range data are dual-frequency (S-band minus X-band) range delay in nanoseconds. For each tracking pass, anywhere from 1 to as many as 100 individual range measurements were available; a composite range delay was constructed by averaging the highest and lowest value from each tracking pass. Since the *maximum* variation in range delay measurements per tracking pass was typically between 2 and 20%, it is considered that the procedure was more than adequate to secure a reasonable daily composite range delay value.

III. The Data Model

Figure 1 provides the correlation between the concurrent range delay and doppler noise pass average data; as is seen, an empirically selected proportionality constant of 5×10^4 Hz s^{-1} provides a very good fit to the data. Figure 2 presents both range delay and doppler noise vs day of year, while Fig. 3 presents the same data vs signal path offset distance (in solar radii). In both Figs. 2 and 3, the range data have been converted to Hz via the proportionality constant (5×10^4 Hz s^{-1}) shown in Fig. 1.

The model shown in Figs. 2 and 3 represents the signal path integration of an electron density model $N_e(r) = 2.21 \times 10^8 r^{-6} + 1.55 \times 10^6 r^{-2.3}$, where the units are cm^{-3}. The coefficient and the radial exponent (-2.3) of the second term was determined by a least squares curve fit to the phase fluction data in Fig. 2 (Refs. 27, 28), while the coefficient of the first term was determined from Viking and Helios phase fluctuation measurements between 2 and 6 solar radii (Fig. 4, from Ref. 30). The radial exponent (-6.0) for the near corona term derives from solar eclipse measurements (Ref. 33). The constant K_2 shown in Figs. 2 and 3 is equal to the speed of light (cm sec^{-1}) times the columnar content (cm^{-3}) per cm of electron density induced signal delay.

The comparison of range delay to doppler noise for the data acquired from November 28, 1976 to December 5, 1976 (day of year 333 to 340) appears to differ somewhat from the comparison over the remainder of the period and hence (this range data) has been marked with a different symbol in the figures. Possible explanations for this difference are (1) a region of enhanced fluctuation-to-density ratio, or less likely (2) systematically erroneous range measurements.

The observations here discussed are columnar quantities; for ease of comparison to other electron density (radial) distribution work, one desires the generating point source electron density distribution. To facilitate the comparison, a closed form approximation of the integral (of the solar wind component of electron density)

$$\int^{R_{s/c}} r^{-(2+\zeta)}\, dR \qquad (1)$$

where

R = signal path

$R_{s/c}$ = Earth-spacecraft distance

r = heliocentric signal distance

is desired. Figure 5 details the appropriate geometrical configuration. Equation (1) is rewritten as:

$$(r_e \sin\alpha)^{-(1+\zeta)} \int_{\alpha-\pi/2}^{\beta-\pi/2+\alpha} (\cos\omega)^{\zeta}\, d\omega \qquad (2)$$

where α = Sun-Earth-Spacecraft angle, β = Earth-Sun-Spacecraft angle, r_e = Earth-Sun distance, and:

$$\omega = \tan^{-1}(R - r_e \cos\alpha / r_e \sin\alpha) \quad (3)$$

A Macluarin series is utilized to expand $(\cos\omega)$

$$(\cos\omega)^{\zeta} \cong 1 + \frac{\omega^2}{2!}(-\zeta) + \frac{\omega^4}{4!}(-1.1\,\zeta) + \cdots \quad (4)$$

After the indicated integration one has:

$$\int^{R_{s/c}} r^{-(2+\zeta)}\,dR = K r_e^{-(1+\zeta)}\,\beta\,(\sin\alpha)^{-(1+\zeta)}\,F(\alpha,\beta) \quad (5)$$

where

$$F(\alpha,\beta) \cong 1 - 0.05\left\{\frac{(\beta - \pi/2 + \alpha)^3 - (\alpha - \pi/2)^3}{\beta}\right\} - 0.00275\left\{\frac{(\beta - \pi/2 + \alpha)^5 - (\alpha - \pi/2)^5}{\beta}\right\} \quad (6)$$

In this work, all data fitting (Eq. 5) makes use of the two independent geometrical parameters α and β, which directly relate to the signal path solar offset distance and signal path length, respectively. Much work in determining electron density distribution has customarily relied on usage of only the dominant geometrical parameter α. Significant errors can result in experimentally determining radial dependence via reliance on only one geometrical parameter (Ref. 34).

It is noteworthy that this electron density model is in good agreement with K-coronameter measurements at $2r_0$ (Refs. 35-37), pulsar time delay measurements at $10\,r_0$ (Refs. 38, 39), and in situ electron density measurements at 1 AU (Ref. 40). The model gives a significantly higher electron density at $10r_0$ than spacecraft range data from Helios 1 and 2 (Ref. 41) and Mariners 6 and 7 (Ref. 23). Table 1 presents various model determinations at $10r_0$.

IV. Discussion

Since at least the late 1960s, the theoretical relationship between columnar phase fluctuation and columnar electron density has been extensively hypothesized, but definitive concurrent measurements of the two parameters have not (previously) been available to test the various hypotheses. Recent efforts in theoretically analyzing the radial dependence of phase fluctuation (Refs. 19, 42) have produced phase fluctuation models which are proportional to the product of density fluctuation and solar wind (radial) velocity times a factor of $r^{0.5}(\sigma_{n_e}(r)\,v\,(r)r^{0.5})$. Under the common assumptions of (1) proportionality between density and density fluctuation, and (2) the conservation of particle flux, such phase fluctuation models are immediately seen to be proportional to $r^{-1.5}$ and hence are independent of the actual radial dependence of electron density.

These theoretically derived phase fluctuation models of Woo and Callahan are not compatible with the concurrent measurements of Viking doppler noise (phase fluctuation) and range (time delay) as presented in this article. In particular, the $r^{-1.5}$ models fail in the near-corona region, where the electron density radial dependence changes from $r^{-2.3}$ to r^{-6}. This can be seen in the near-corona region of Fig. 3 and in Fig. 4, where the phase fluctuation data are well fit by a model of functional form r^{-5} ($\propto \int r^{-6}\,dR$). Clearly, a model of the form $r^{-1.5}$ could not reasonably fit these data.

In way of possible explanation of this incompatibility, it is to be noted that analyses performed much earlier and which employed geometrical optics (Refs. 11, 14, and 21) predicted this now observed radial proportionality between signal phase fluctuation and columnar electron density, under the very reasonable assumption of a linear transverse fluctuation scale ($L_t = Kr$), as would directly be expected from a radially outflowing solar wind (Ref. 21).

Acknowledgment

The authors wish to thank D. L. Cain and P. S. Callahan, of the Jet Propulsion Laboratory, for their review of this paper, and the many excellent comments and suggestions which they provided. The authors are particularly indebted to Professor G. L. Tyler, of Stanford University, for his comprehensive review of and assistance provided to this article.

References

1. Intriligator, D. S., and Wolfe, J. H., "Preliminary Power Spectra of the Interplanetary Plasma," *Astrophys. J. Let.*, Vol. 162, L187, 1970.

2. Goldstein, B., and Sisco, G. L., "Spectra and Cross Spectra of Solar Wind Parameters from Mariner 5," *Solar Wind*, NASA SP-308, p. 506, 1972.

3. Unti, T., Neugebauer, M., and Goldstein, B. E., "Direct Measurements of Solar Wind Fluctuations Between 0.0048 and 13.3 Hz," *Astrophys. J.*, Vol. 180, p. 591, 1973.

4. Slee, O. B., "Observations of the Solar Corona Out to 100 Solar Radii," *Mon. Not. R. Astr. Soc.*, Vol. 123, p. 16, 1961.

5. Slee, O. B., "The Outer Solar Corona During the Declining Portion of The Solar Activity Cycle," *Planet. Space Sci.*, Vol. 14, p. 255, 1966.

6. Okoye, S. E., and Hewish, A., "Irregularities of Plasma Density in the Solar Neighborhood," *Mon. Not. R. Astr. Soc.*, Vol. 137, p. 18, 1967.

7. Cohen, M. H., Gundermann, E. J., Hardibeck, H. E., and Sharp, L. E., "Interplanetary Scintillations II. Observations," *Astrophys. J.*, Vol. 147, No. 2, p. 449, 1967.

8. Cohen, M. H., and Gundermann, E. J., "Interplanetary Scintillations IV. Observations Near the Sun," *Astrophys. J.*, Vol. 155, No. 2, p. 645, 1969.

9. Salpeter, E. E., "Interplanetary Scintillations. I. Theory," *Astrophys. J.*, Vol. 147, No. 2, p. 433, 1967.

10. Cronyn, W. M., "The Analysis of Radio Scattering and Space Probe Observations of Small Structure in The Interplanetary Medium," *Astrophys. J.*, Vol. 161, No. 2, p. 755, 1970.

11. Jokipii, J. R., and Hollweg, J. V., "Interplanetary Scintillations and the Structure of Solar Wind Fluctuations," *Astrophys. J.*, Vol. 160, No. 2, p. 745, 1970.

12. Hewish, A., and Symonds, M. D., "Radio Investigation of the Solar Plasma," *Planet. Space Sci.*, Vol. 17, p. 313, 1969.

13. Hewish, A., "Observations of the Solar Plasma Using Radio Scattering and Scintillation Methods," *Solar Wind, NASA SP-308*, p. 477, 1972.

14. Little, L. T., "Small Scale Plasma Irregularities in the Interplanetary Medium," *Astron. & Astrophys.*, Vol. 10, p. 301, 1971.

15. Readhead, A. C. S., "Interplanetary Scintillation of Radio Sources at Metre Wavelengths – II," *Mon. Not. Astr. Soc.*, Vol. 155, p. 185, 1971.

16. Rickett, B. J., "Power Spectrum of Density Irregularities in the Solar Wind Plasma," *J. Geophys. Res.*, Vol. 78, No. 10, 1543, 1973.

17. Chang, H., "Analysis of Dual Frequency Observations of Interplanetary Scintillation Taken by the Pioneer 9 Spacecraft," Ph. D. Thesis, Stanford University, Stanford, Calif. 1976.

18. Rockwell, R. S., "An Empirical Spectral Bandwidth Model for Superior Conjunction," *DSN Progress Report 42-43*, Jet Propulsion Laboratory, Pasadena, Calif., p. 216, Feb. 15, 1978.

19. Woo, R., "Radial Dependence of Solar Wind Properties Deduced from Helios 1/2 and Pioneer 10/11 Radio Scattering Observations," *Astrophys. J.*, Vol. 219, p. 727, 1978.

20. Woo, R., and Armstrong, J. W., "Spacecraft Radio Scattering Observations of Electron Density Fluctuations in the Solar Wind," *J. Geophys. Res.*, Vol. 84 No. A12, p. 7288, 1979.

21. Hollweg, J. V., "A Statistical Ray Analysis of the Scattering of Radio Waves by the Solar Corona," *Astronom. J.*, Vol. 73, No. 10, p. 927, 1968.

22. Goldstein, R. M., *The Superior Conjunction of Mariner IV*, Technical Report 32-1092, Jet Propulsion Laboratory, Pasadena, Calif., 1967.

23. Muhleman, D. O., Esposito, P. B., and Anderson, J. D., "The Electron Density Profile of the Outer Corona and the Interplanetary Medium from Mariner 6 and Mariner 7 Time Delay Measurements," *Astrophys. J.*, Vol. 211, p. 943, 1977.

24. Callahan, P. S., "Columnar Content Measurements of the Solar-Wind Turbulence Near the Sun," *Astrophys. J.*, Vol. 199, p. 227, 1975.

25. Berman, A. L., and Rockwell, S. T., "Analysis and Prediction of Doppler Noise During Solar Conjunctions," *DSN Progress Report 42-30*, p. 231, Jet Propulsion Laboratory, Pasadena, Calif., Dec. 15, 1975.

26. Berman, A. L., and Wackley, J. A., "Doppler Noise Considered as a Function of the Signal Path Integration of Electron Density," *DSN Progress Report 42-33*, p. 159, June 15, 1976.

27. Berman, A. L., and Wackley, J. A., "Viking S-Band Doppler RMS Phase Fluctuations Used To Calibrate the Mean 1976 Equatorial Corona," *DSN Progress Report 42-38*, p. 152, Apr. 15, 1977.

28. Berman, A. L., Wackley, J. A., Rockwell, S. T., and Kwan, M., "Viking Doppler Noise Used To Determine the Radial Dependence of Electron Density in the Extended Corona," *DSN Progress Report 42-38*, p. 167, Apr. 15, 1977.

29. Berman, A. L., "Electron Density in the Extended Corona – Two Views," *DSN Progress Report 42-41*, p. 135, Jet Propulsion Laboratory, Pasadena, Calif., Oct. 15, 1977.

30. Berman, A. L., "Electron Density and Doppler RMS Phase Fluctuation in the Inner Corona," *DSN Progress Report 42-44*, p. 172, Jet Propulsion Laboratory, Pasadena, Calif., Apr. 15, 1978.

31. Berman, A. L., "Phase Fluctuation Spectra: New Radio Science Information To Become Available in the DSN Tracking System Mark III-77," *DSN Progress Report 42-40*, p. 134, Jet Propulsion Laboratory, Pasadena, Calif., Aug. 15, 1977.

32. Koehler, R. L., "Radio Propagation Measurements of Pulsed Plasma Streams from the Sun Using Pioneer Spacecraft," *J. Geophys. Res.*, Vol. 78, No. 15, p. 4883, 1968.

33. Anderson, J. D., Esposito, P. B., Martin W., and Thornton, C. L., "Experimental Test of General Relativity Using Time-Delay Data from Mariner 6 and Mariner 7," *Astrophys. J.*, Vol. 200, p. 221, 1975.

34. Berman, A. L., "Precise Extraction of Geometrical Dependence from Solar Wind Columnar Turbulence Measurements," *DSN Progress Report 42-50*, p. 110, Jet Propulsion Laboratory, Pasadena, Calif., Apr. 15, 1979.

35. Hansen, R. T., Garcia, C. J., Hansen, S. F., and Loomis, H. C., "Brightness Variations of the White Light Corona During the Years 1964-1967," *Sol. Phys.*, Vol. 7, 1969.

36. Saito, K., "A Non-Spherical Axisymmetric Model of the Solar K Corona of the Minimum Type," *Ann. Tokyo Astron. Observ.*, No. 2 Vol. XII, 1970.

37. Saito, K., Poland, A. I., and Munro, R. H., "A Study of the Background Corona Near Solar Minimum," *Sol. Phys.*, Vol. 55, 1977.

38. Counselman, III., C. C., and Rankin, J. M., "Density of the Solar Corona from Occultations of NP0532," *Astrophys. J.*, Vol. 175, 1972.

39. Weisberg, J. M., Rankin, J. M., Payne, R. R., and Counselman III., C. C., "Further Changes in the Distribution of Density and Radio Scattering in the Solar Corona," *Astrophys. J.*, Vol. 209, p. 252, 1976.

40. Diodato, L., Moreno, G., Signorini, C., and Ogilvie, K. W., "Long-Term Variations of the Solar Wind Proton Parameters," *J. Geophys. Res.*, Vol. 79, No. 34, p. 5095, 1974.

41. Esposito, P. B., Edenhofer, P., and Lüneburg, E., "Solar Corona Electron Density Distribution," *J. Geophys. Res.*, Vol. 85, No. A7, p. 3414, 1980.

42. Callahan, P. S., "A First Principles Derivation of Doppler Noise Expected from Solar Wind Density Fluctuations," *DSN Progress Report 42-42*, p. 42, Jet Propulsion Laboratory, Pasadena, Calif., Dec. 15, 1977.

Table 1. Electron density models evaluated at $10r_0$

Source	$N_e(10r_0)$, electrons cm^{-3}	Type of experiment
This article	8000	Dual-frequency range
Ref. 41	4500	Helios 1 and 2 S-band range
Ref. 23	5600	Mariner 7 S-band range
Ref. 39	8000	Pulsar time delay
Ref. 38	8400	Pulsar time delay

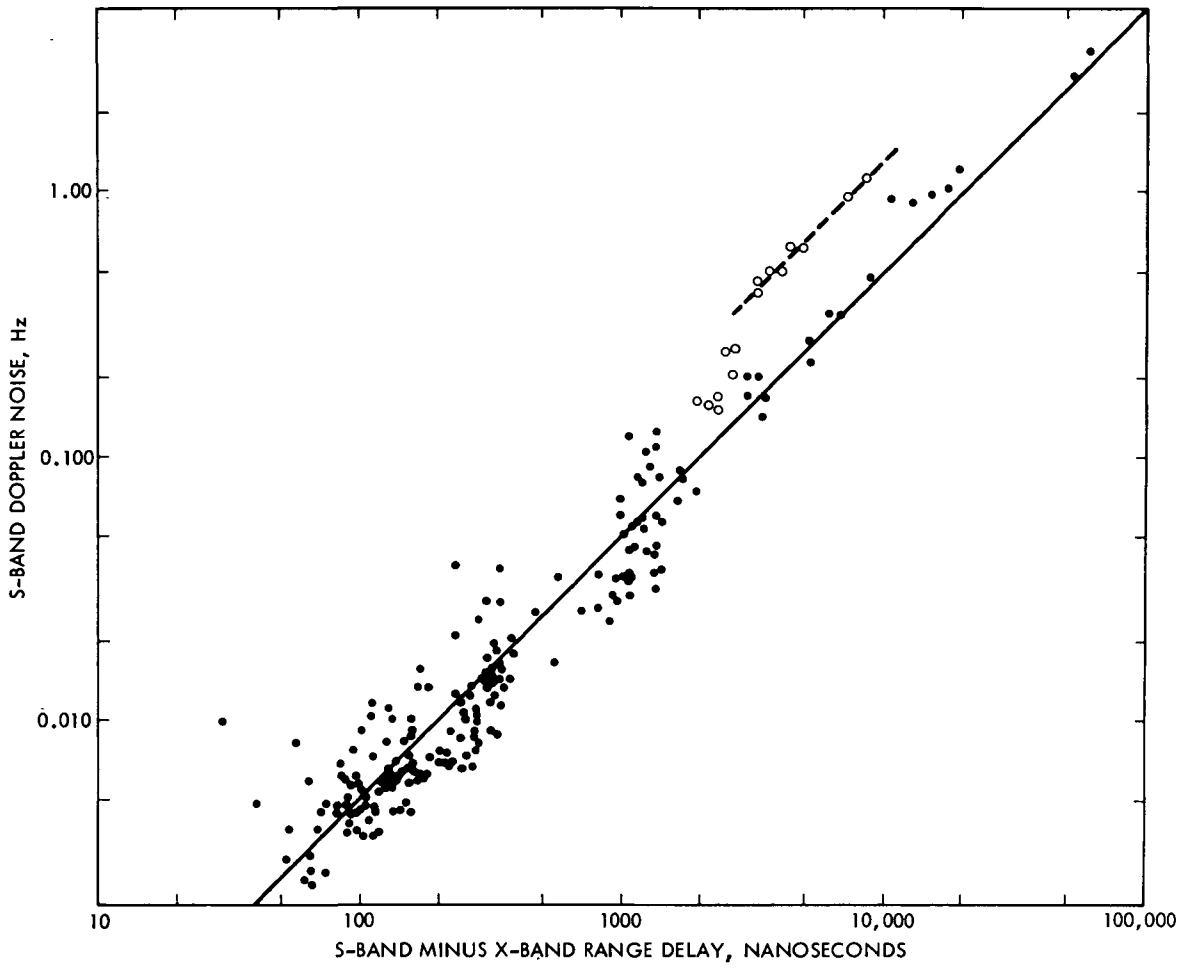

Fig. 1. Correlation between σ_d = 13-cm signal phase fluctuation and integrated electron density. The solid data points are from July 2 to November 27, 1976, and December 6 to December 20, 1976, while the hollow points are from November 28, to December 5, 1976. The solid line represents the proportionality constant 5×10^4 Hz/s, while the dashed line represents 1.3×10^5 Hz/s

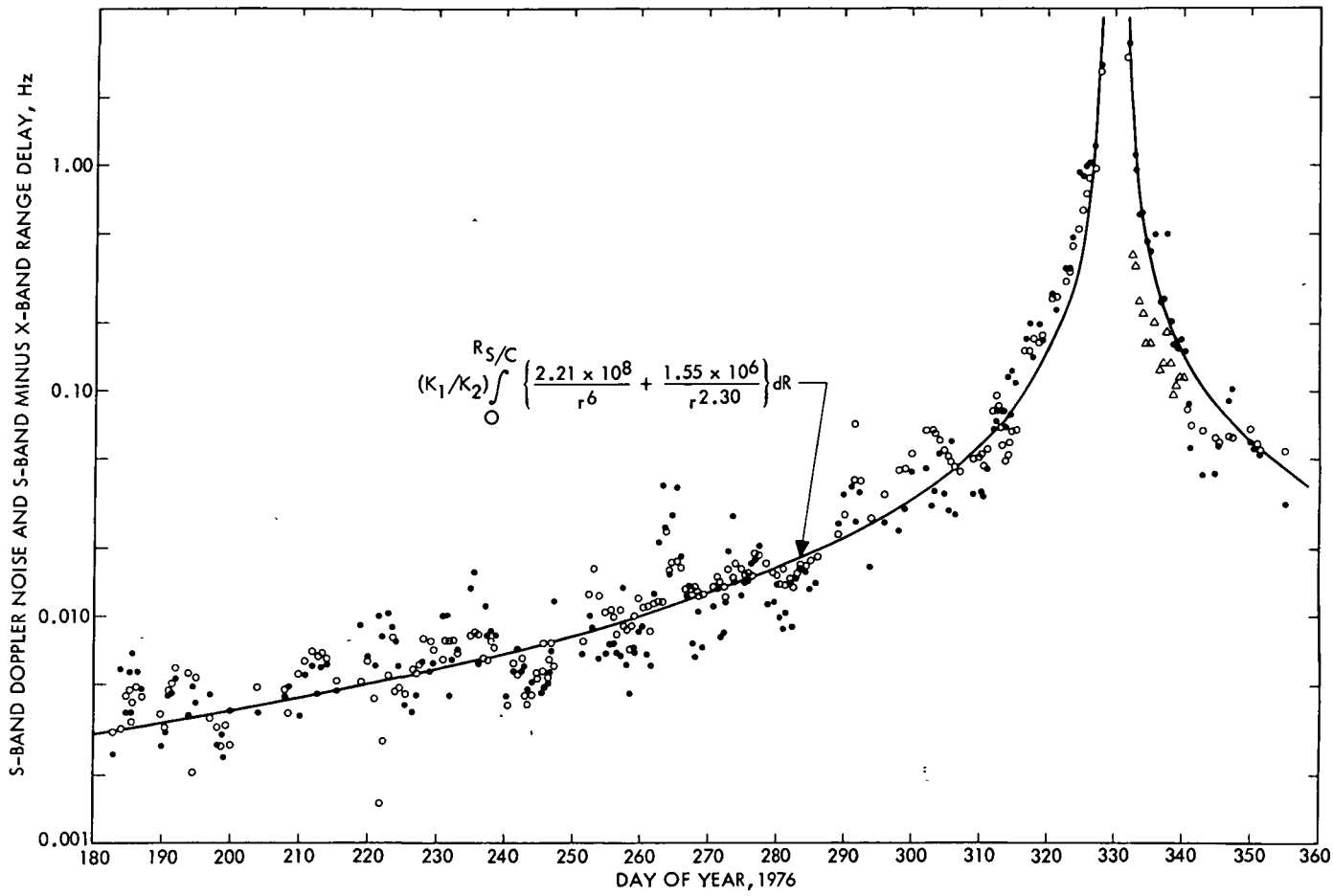

Fig. 2. Signal phase fluctuation and integrated electron density vs day of year, 1976. The solid points are σ_d = 13-cm Doppler noise in Hz, while hollow points are dual-frequency range in nanoseconds multiplied by the proportionality constant $K_1 = 5 \times 10^4$ Hz/s. Hollow circles are data from July 2 to November 27, 1976, and December 6 to December 20, 1976, while hollow triangles are data from November 28 to December 5, 1976. The constant $K_2 = 3.93 \times 10^{21}$ cm^{-2}s^{-1} is the number of columnar electrons per second of dual-frequency range delay

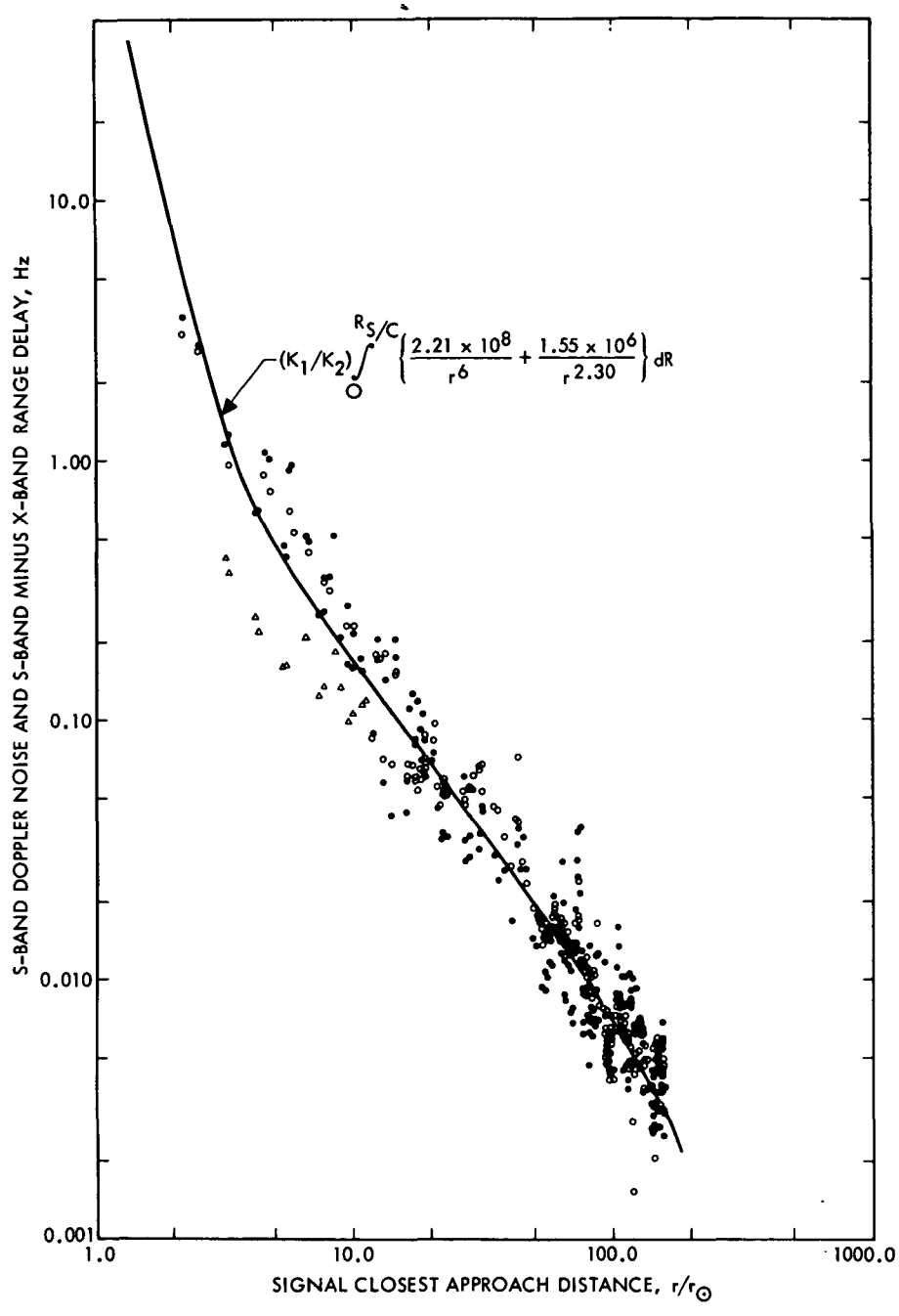

Fig. 3. Signal phase fluctuation and integrated electron density vs solar offset distance. The solid points are σ_d = 13-cm Doppler noise in Hz, while the hollow points are dual-frequency range in nanoseconds multiplied by the proportionality constant K_1 = 5×10^4 Hz/s. Hollow circles are data from July 2 to November 27, 1976, and December 6 to December 20, 1976, while hollow triangles are data from November 28 to December 5, 1976. The constant $K_2 = 3.93 \times 10^{21}$ cm^{-2}s^{-1} is the number of columnar electrons per second of dual-frequency range delay

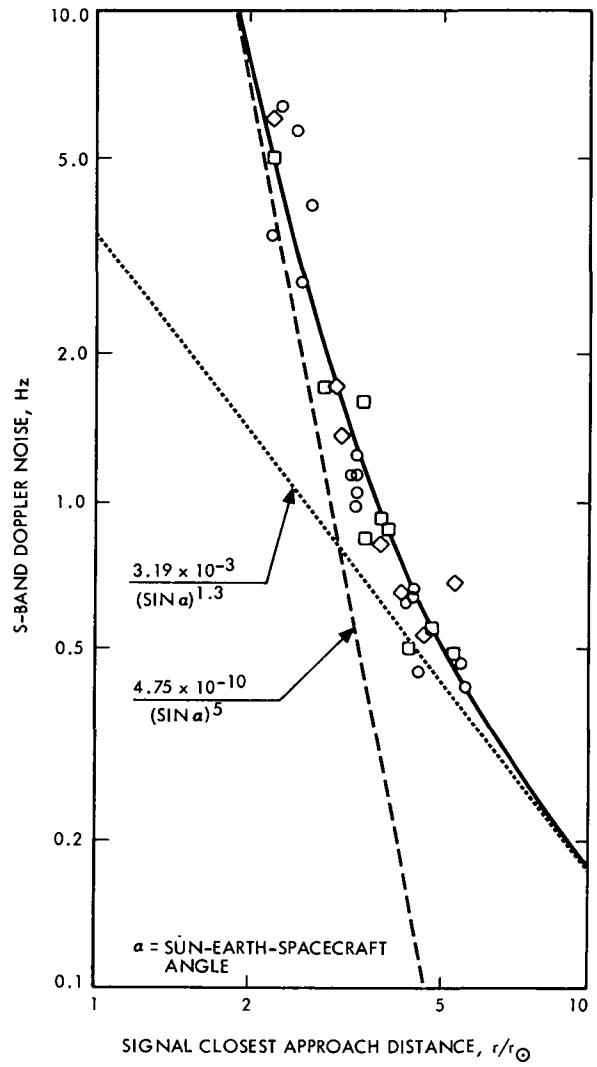

Fig. 4. Signal phase fluctuation in the inner corona. Circles are data from the Viking 1976 solar conjunction, diamonds are data from the Helios 2 1976 solar conjunction, and squares are data from the Helios 1 1975 solar conjunction

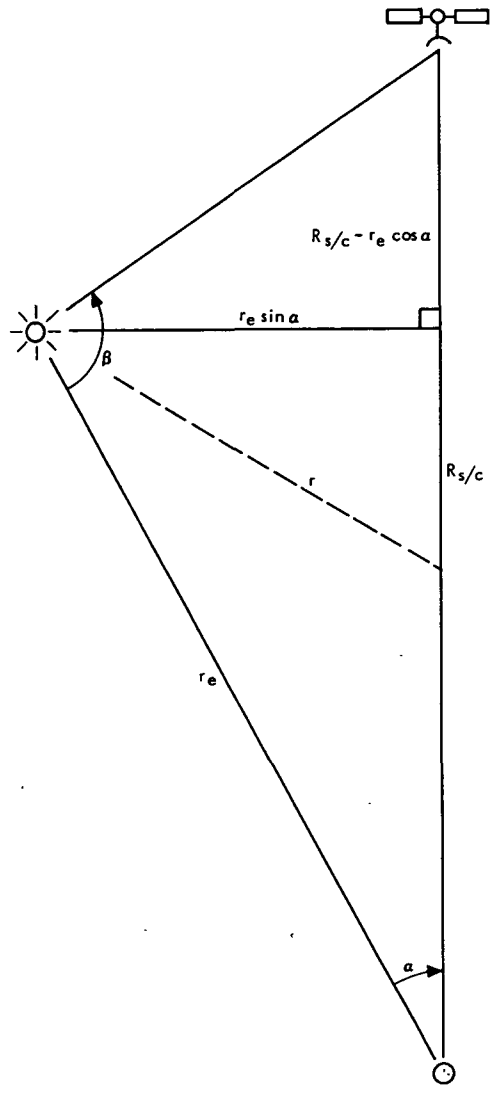

Fig. 5. Sun-Earth-Spacecraft geometrical configuration. r = heliocentric distance to signal path, r_e = Earth-Sun distance, $R_{s/c}$ = Earth-Spacecraft distance, α = Sun-Earth-Spacecraft angle, and β = Earth-Sun-Spacecraft angle